Nonlinear Dyn (2015) 82:2069–2079
DOI 10.1007/s11071-015-2300-1

ORIGINAL PAPER

A new six-term 3-D chaotic system with fan-shaped Poincaré maps

Jinmei Liu · Qiang Qu · Guanjing Li

Received: 8 October 2014 / Accepted: 24 July 2015 / Published online: 1 August 2015

Abstract A new three-dimensional chaotic system with fan-shaped Poincaré maps is proposed. Based on merely six terms, the system is easy to implement. Its dynamic behaviors, such as equilibrium points, Poincaré maps, power spectra, Lyapunov exponent spectra, bifurcation diagrams and forming mechanism, are analyzed theoretically and numerically. Results of theoretical analyses and numerical simulations indicate that the proposed system possesses complex chaotic attractors. Its equilibrium points are unstable, and the system can keep chaotic when its parameters vary in a wide domain. Furthermore, circuit simulations of the system are discussed. The results of numerical simulations and circuit simulations coincide very well. By virtue of its complex dynamic behaviors and wide-range parameters, the system can be adopted in some application fields where wide-range parameters and complex behaviors are usually preferred, such as secure communication, data encryption, information hiding.

Keywords Chaos · Attractors · Poincaré map · Fan-shaped

J. Liu (✉) · G. Li
College of Information Science and Technology, Jinan University, Guangzhou 510632, China
e-mail: jinmei_liu@126.com

Q. Qu
Automobile Electronic Technology Department, Shandong Transport Vocational College, Weifang, China

1 Introduction

Chaos, known by its deterministic, unpredictability and extremely sensitive dependence on initial conditions, stems from nonlinear systems [1]. Since Lorenz discovered a three-dimensional autonomous chaotic system [2] with quadratic terms, many chaotic systems have been proposed and studied [6–19]. Among the existing chaotic systems, some belong to three dimensions and others belong to four or higher dimensions. Because of their simple algebraic structures for easy implementation, some three-dimensional chaotic systems are welcome in many engineering application fields, for instance, the Rössler system [3], the Genesio and Tesi system [4], the Sprott system [5,6], the Chen system [7] and Lü system [8], the Liu system [9] and so on. By now, Chaos can be applied in many areas, such as mechanics [20], flow dynamics [21], biomedical engineering [22], communications [23] and information security [24]. Due to the widely applications of chaotic systems in various fields, it is meaningful to design and study new chaotic systems that are simple to implement.

In our research, we designed a new three-dimensional chaotic system with only six terms. The system is not only convenient to realize, but also possess peculiar fan-shaped Poincaré maps. Moreover, the system can keep chaotic in a wide range of parameters, so it would be a good candidate for some engineering fields such as secure communications, information security, etc.

This paper is organized as follows: Mathematic model, dynamical features of the new three-dimensional chaotic system are briefly introduced in Sect. 2; dynamical behaviors such as equilibrium points, Poincaré map, power spectra, Lyapunov exponent spectra and bifurcation diagrams of the system are discussed in Sect. 3; forming mechanism of the system is described in Sect. 4. Circuit simulations are discussed in Sect. 5. Section 6 is the conclusions.

2 A new 3-D chaotic system

A new three-dimensional chaotic system is established by the following equations.

$$\begin{cases} \dot{x} = -ax + by \\ \dot{y} = -xz \\ \dot{z} = cx^2 + xy - d \end{cases} \tag{1}$$

where a, b, c and d are the system parameters. In the equation, nonlinear terms are formed by one cross-product and one square term. Figure 1 shows phase diagrams of the system (1) when $(a, b, c, d) = (1, 2, 1, 3)$, with initial states $(x_0, y_0, z_0) = (0.1, 0.1, 0.1)$. Figure 2 shows phase diagrams of the system (1) when $(a, b, c, d) = (1, 5, 1, 3)$. From Figs. 1 and 2, it can be seen that the system exhibits complex and strange attractors. Figures 3 and 4, respectively, show the Poincaré maps projected in the y–z, x–z and x–y plane with different parameters.

For system (1), $\nabla V = \frac{\partial \dot{x}}{\partial x} + \frac{\partial \dot{y}}{\partial y} + \frac{\partial \dot{z}}{\partial z} = -a$.

In order to ensure the dissipation of the system, it is required that $-a < 0$. Then the system can contract at an exponential rate e^{-at}. When a is positive, the system converges at a rate of e^{-at}. Therefore, each volume cell containing the system orbits finally converges into zero as $t \to \infty$. In order to make the motion of the system (1) settle onto an attractor, $a > 0$ is required.

3 Some properties of the new chaotic system

3.1 Symmetry

The system (1) is symmetrical under the transformation $(x, y, z) \to (-x, -y, z)$. Besides, the system (1) is invariant under the transformation $(x, y, z, a, b, c, d) \to (x, -y, -z, a, -b, -c, -d)$.

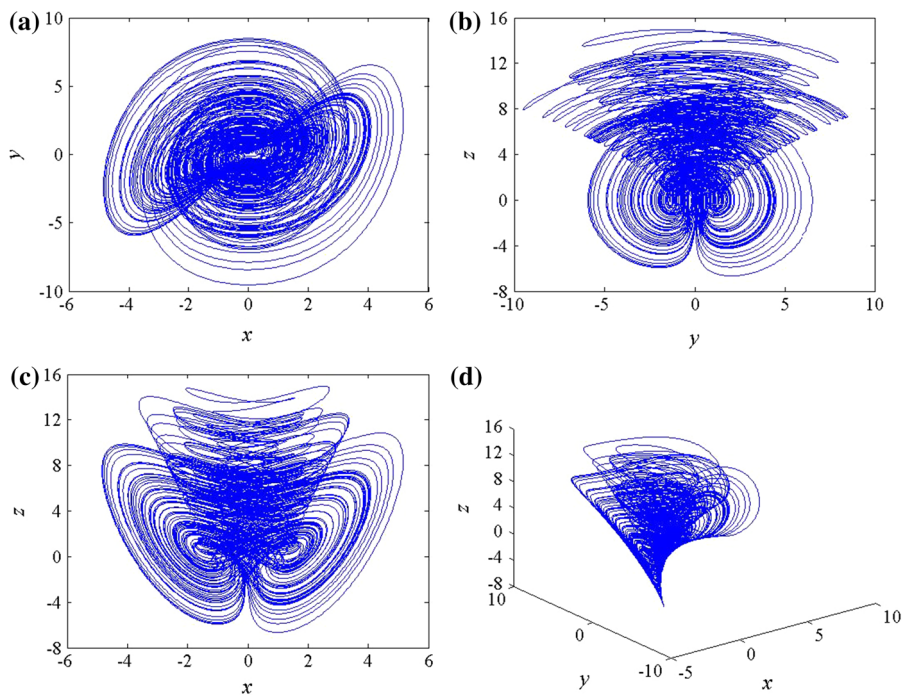

Fig. 1 Phase diagrams when $(a, b, c, d) = (1, 2, 1, 3)$: **a** x–y, **b** y–z, **c** x–z, **d** x–y–z

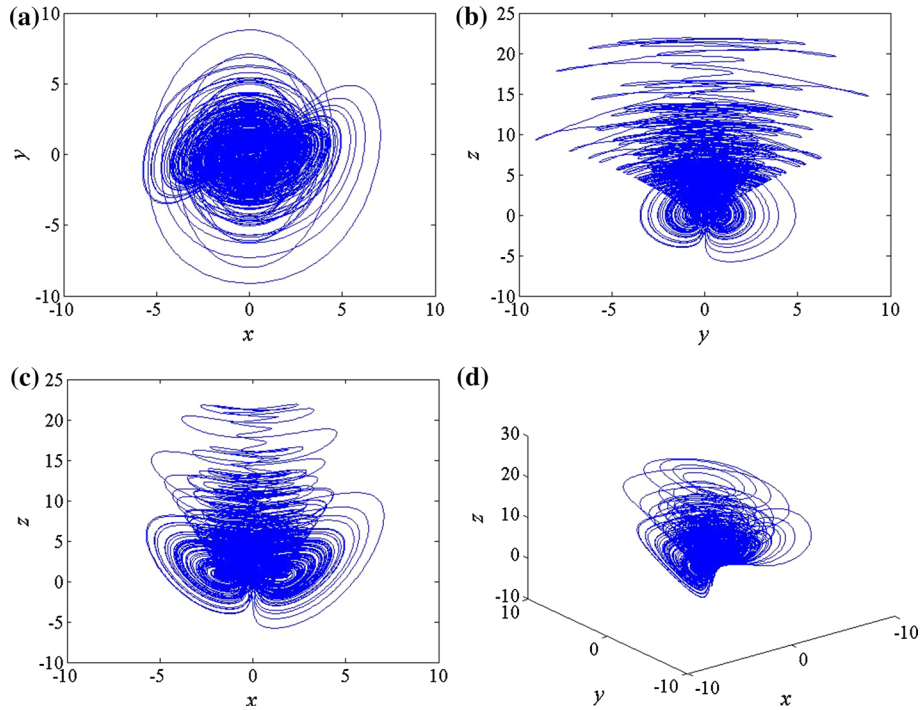

Fig. 2 Phase diagrams when $(a, b, c, d) = (1, 5, 1, 3)$: **a** x–y, **b** y–z, **c** x–z, **d** x–y–z

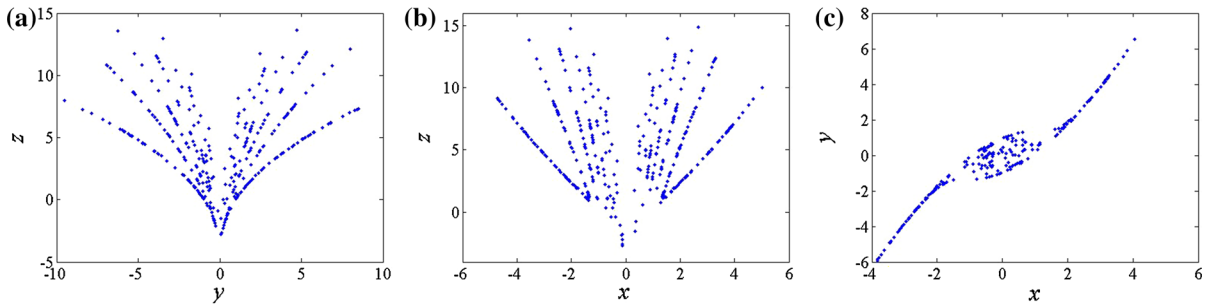

Fig. 3 Poincaré map when $(a, b, c, d) = (1, 2, 1, 3)$: **a** $x = 0$, **b** $y = 0$, **c** $z = 0$

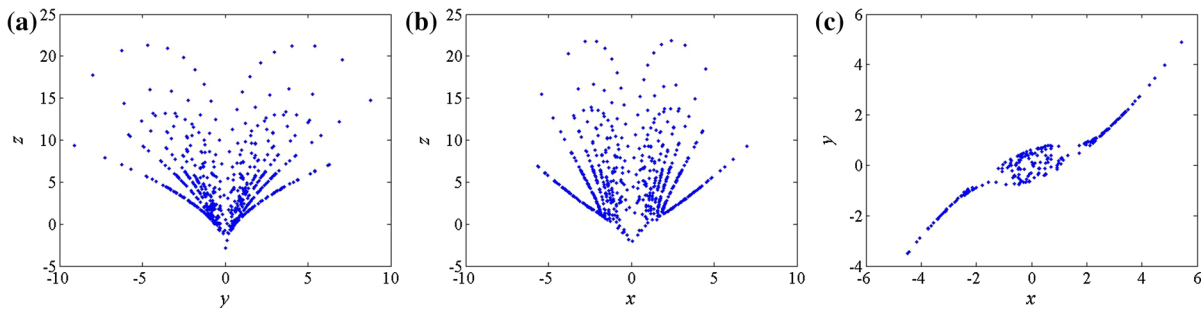

Fig. 4 Poincaré map when $(a, b, c, d) = (1, 5, 1, 3)$: **a** $x = 0$, **b** $y = 0$, **c** $z = 0$

3.2 Equilibrium points and stability

For calculating equilibria, let

$$\begin{cases} -ax + by = 0 \\ -xz = 0 \\ cx^2 + xy - d = 0 \end{cases} \tag{2}$$

When $\frac{bd}{a+bc} > 0$, the system possesses two equilibrium points $E_1\left(\sqrt{\frac{bd}{a+bc}}, \frac{a}{b}\sqrt{\frac{bd}{a+bc}}, 0\right)$ and $E_2\Big(-\sqrt{\frac{bd}{a+bc}}, -\frac{a}{b}\sqrt{\frac{bd}{a+bc}}, 0\Big)$.

For an equilibrium point $E(x, y, 0)$, its Jacobian matrix is

$$J_E = \begin{bmatrix} -a & b & 0 \\ 0 & 0 & -x \\ 2cx + y & x & 0 \end{bmatrix} \tag{3}$$

Let $|\lambda I - J_E| = 0$, we get

$$\lambda^3 + a\lambda^2 + x^2\lambda + \left[(a + 2bc)\, x^2 + bxy\right] = 0 \tag{4}$$

For $E_1\left(\sqrt{\frac{bd}{a+bc}}, \frac{a}{b}\sqrt{\frac{bd}{a+bc}}, 0\right)$ and $E_2\Big(-\sqrt{\frac{bd}{a+bc}}, -\frac{a}{b}\sqrt{\frac{bd}{a+bc}}, 0\Big)$, we have

$$\lambda^3 + a\lambda^2 + \frac{bd}{a + bc}\lambda + 2bd = 0 \tag{5}$$

According to criterion, Eq. (5) has one negative real root and one pair of complex conjugate roots with positive real part if and only if

$$\frac{abd}{a + bc} - 2bd < 0, \quad 2bd > 0 \tag{6}$$

So, when $bd > 0, bc > 0, a > -bc$, the equilibrium points E_1 and E_2 are unstable. According to Sect. 2, $a > 0$ should be satisfied. Therefore, we can get the following remark.

Remark 3.1 Equation (6) is satisfied and the E_1 and E_2 are all unstable saddle points when either of the following conditions is satisfied:

(1) $a > 0, b > 0, c > 0, d > 0$.
(2) $a > 0, b < 0, c < 0, d < 0$.

Theorem 3.1 *When $a > 0, b > 0, c > 0, d > 0$ or $a > 0, b < 0, c < 0, d < 0$, the vector fields of the system satisfy the conditions for generating chaos.*

Proof Let $A = a^2 - \frac{3bd}{a+bc}$, $B = \frac{abd}{a+bc} - 18bd$, $C = \left(\frac{bd}{a+bc}\right)^2 - 6abd$, $D = B^2 - 4AC$, $U = Aa + 1.5(-B + \sqrt{D})$, $V = Aa + 1.5(-B - \sqrt{D})$.

We get the following solutions of Eq. (5):

$$\begin{cases} \lambda_1 = \frac{-a - \left(\sqrt[3]{U} + \sqrt[3]{V}\right)}{3} \\ \lambda_{2,3} = \frac{-a + 0.5\left(\sqrt[3]{U} + \sqrt[3]{V}\right)}{3} \pm j\frac{\sqrt{3}\left(\sqrt[3]{U} - \sqrt[3]{V}\right)}{6} \end{cases} \tag{7}$$

According to Shil'nikov theorem, for the eigenvalues γ and $\sigma \pm j\omega$, the vector fields of the system satisfy the conditions for generating chaos if $\gamma\sigma < 0$ and $|\gamma| > |\sigma|$. Here, let $W = \sqrt[3]{U} + \sqrt[3]{V}$, then

$$\begin{cases} \gamma = \frac{-a - W}{3} \\ \sigma = \frac{-a + 0.5W}{3} \end{cases} \tag{8}$$

In fact, when $a > 0, b > 0, c > 0, d > 0$ or $a > 0, b < 0, c < 0, d < 0$, we obtain

$$Aa + 1.5(-B) = a^3 + \frac{22.5a + 27bc}{a + bc}bd > 0 \tag{9}$$

Then, we can get $U > 0$ and $|U| > |V|$. Therefore, $W = \sqrt[3]{U} + \sqrt[3]{V} > 0$. According to Eq. (8), we have $|\gamma| > |\sigma|$. That is to say, when $a > 0, b > 0, c > 0, d > 0$ or $a > 0, b < 0, c < 0, d < 0$, the vector fields of the system (1) satisfy the conditions for generating chaos. The proof is finished.

3.3 Lyapunov exponents and Lyapunov dimension

Lyapunov exponent is a quantity that indicates the average exponential rates of divergence or convergence of adjacent orbits in phase space. If a system is of one or more positive Lyapunov exponents, it is proved to be chaotic. When $a > 0, b > 0, c > 0, d > 0$ or $a > 0, b < 0, c < 0, d < 0$, the system has at least one positive Lyapunov exponent.

We calculate the Lyapunov exponents using the Wolf algorithm. When $(a, b, c, d) = (1, 2, 1, 3)$, the Lyapunov exponents are $\lambda_{L1} = 0.4135$, $\lambda_{L2} = -0.0006$, $\lambda_{L3} = -1.4129$. Its Lyapunov dimension

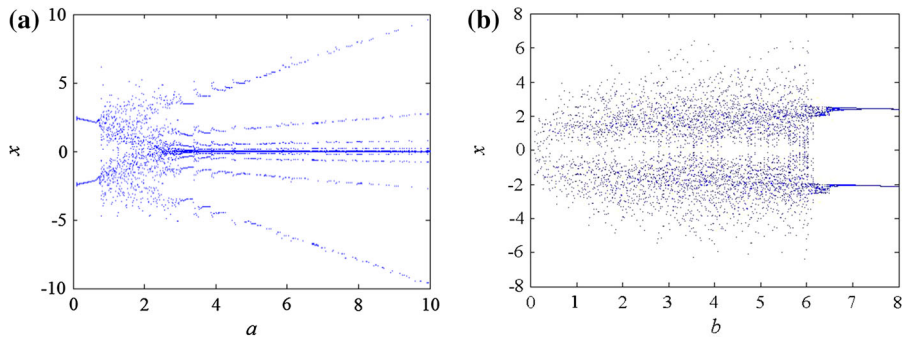

Fig. 5 Bifurcation diagrams: **a** versus a, **b** versus b

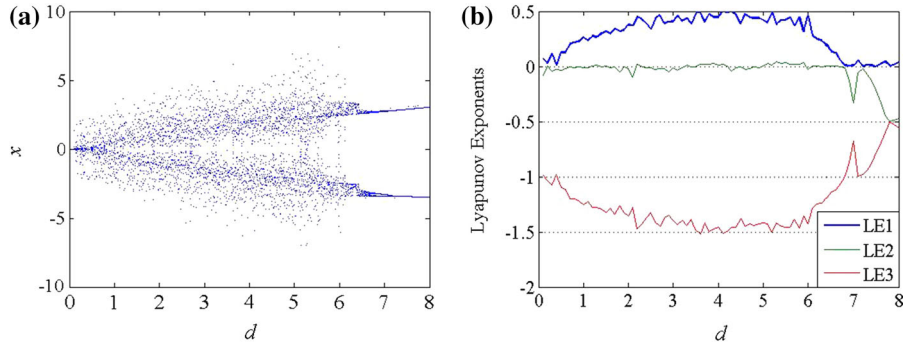

Fig. 6 Bifurcation diagram and Lyapunov exponent spectrum versus d: **a** bifurcation diagram, **b** Lyapunov exponent spectrum

is 2.2922 . When $(a, b, c, d) = (1, 5, 1, 3)$, the Lyapunov exponents are $\lambda_{L1} = 0.4845$, $\lambda_{L2} = -0.0021$, $\lambda_{L3} = -1.4824$. Its Lyapunov dimension is 2.3254 . The attractor of the system (1) is of fraction dimension.

Figure 5a shows the bifurcation diagram of the system (1) versus a with $(b, c, d) = (2, 1, 3)$; Fig. 5b shows the bifurcation diagram versus b with $(a, c, d) = (1, 1, 3)$. Besides, with different ratio of a and b, the system shows the strange-shaped attractors with different layers. This is obvious according to the difference between Figs. 1 and 2.

Figure 6a, b shows the bifurcation diagram and Lyapunov exponent spectrum of the system versus d with $(a, b, c) = (1, 2, 1)$.

3.4 Time-domain waveform and frequency spectrum

When $(a, b, c, d) = (1, 2, 1, 3)$, we get a waveform $x(t)$ of the chaotic system (1) shown in Fig. 7a and its frequency spectrum Log$|x|$ shown in Fig. 7b. We can see from Fig. 7 that the system exhibits complex time behaviors and the bandwidth is about 0–15 Hz.

4 Forming mechanisms of the system

In order to reveal the forming mechanisms of the dynamical system, we add a control parameter u to the system:

$$\begin{cases} \dot{x} = -ax + by \\ \dot{y} = -xz + u \\ \dot{z} = cx^2 + xy - d \end{cases} \tag{10}$$

We set $(a, b, c, d) = (1, 2, 1, 3)$ for the following analyses. When $u = -1.5$, one half part of the original attractors is generated as shown in Fig. 8; when $u = 1.5$, another half part is obtained as illustrated in Fig. 9. That is, Fig. 1 is separated into Figs. 8 and 9 by varying the control parameter u.

Figure 10 demonstrates the dynamical behavior development of the controlled system with $(a, b, c, d) = (1, 2, 1, 3)$.

When $|u| \leq 1.62$, the system shows complex orbits and chaotic behaviors.

When $1.63 \leq |u| \leq 2.57$, the system demonstrates period-doubling bifurcations.

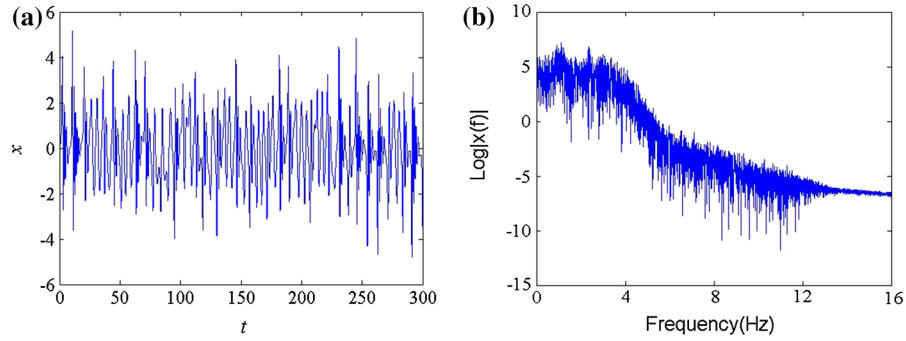

Fig. 7 Waveform and frequency spectrum of x: **a** waveform, **b** spectrum

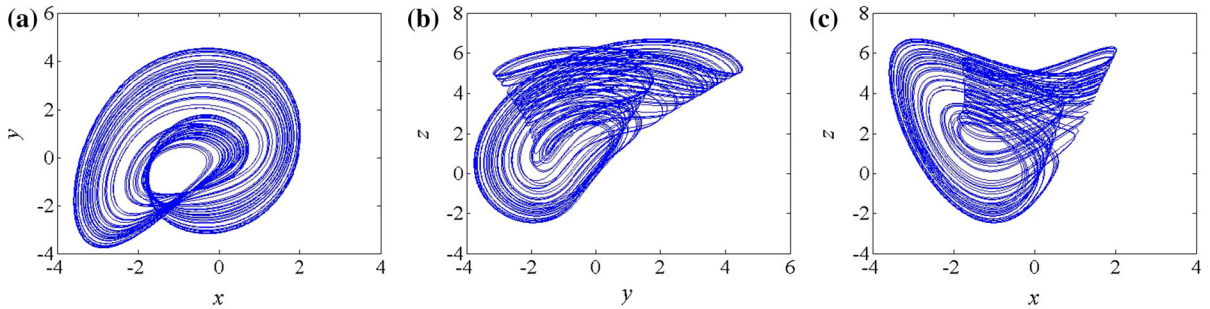

Fig. 8 A half part of attractor when $u = -1.5$: **a** x–y, **b** y–z, **c** x–z

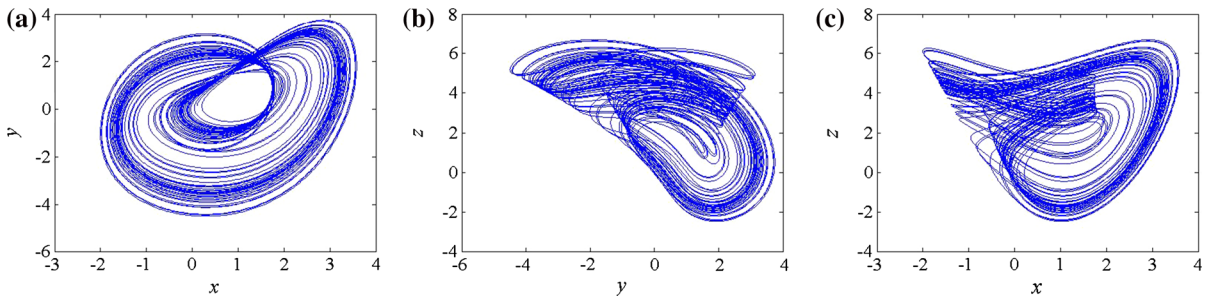

Fig. 9 Another half part of attractor when $u = 1.5$: **a** x–y, **b** y–z, **c** x–z

When $2.58 \leq |u| \leq 7.1$, the system orbit becomes a limit cycle.

When $|u| > 7.24$, the system orbit converges to a point.

To be more specific, bifurcation diagram of the controlled system versus u is shown in Fig. 11, where the dynamical features of the system are evident with different u.

5 Circuit simulation of the system

In order to implement the system (1) with analog integrated operational amplifiers and other electronic elements, the system orbits should be roughly confined into $(-14, 14)$. We can see from Fig. 1 that the orbits of system (1) exceed $(-14, 14)$. Therefore, we construct the following system:

$$\begin{cases} \dot{x} = -ax + by \\ \dot{y} = -kxz \\ \dot{z} = ckx^2 + kxy - d/k \end{cases} \tag{11}$$

where $k \neq 0$. Obviously, the system (11) is a shrink version of the system (1) and orbits of the two systems are of the same shape. More specifically, the orbits of the system (11) are $1/k$ times those of the system (1).

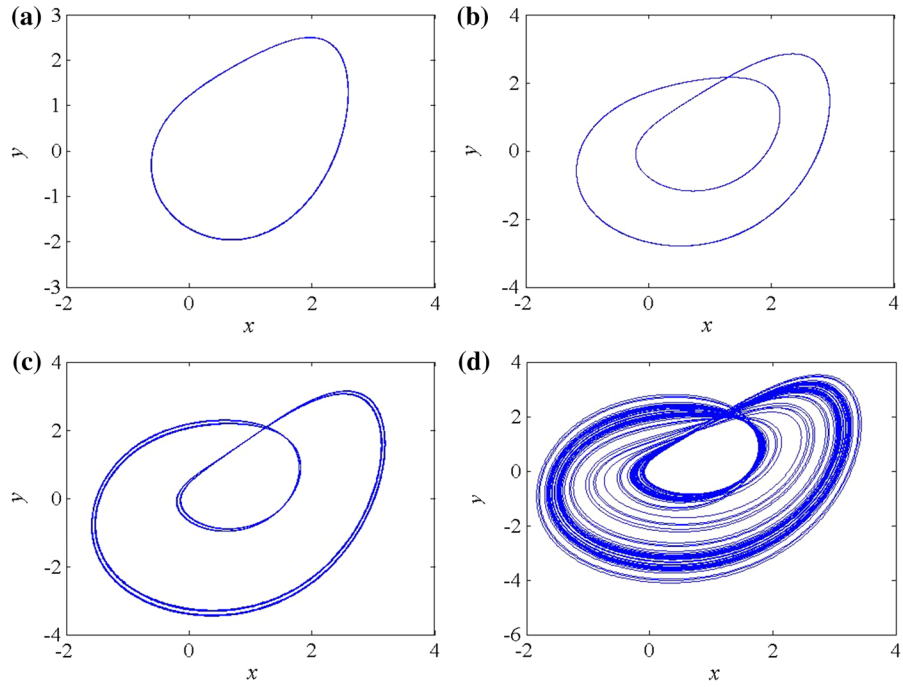

Fig. 10 Phase diagrams on the x–y plane of the controlled system: **a** $u = 2.7$, **b** $u = 2.2$, **c** $u = 1.64$, **d** $u = 1.62$

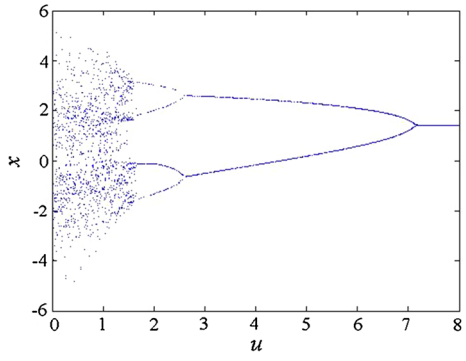

Fig. 11 Bifurcation diagram of the controlled system versus u

We use the Multisim 11 to do circuit simulation. When $(a, b, c, d) = (1, 2, 1, 3)$, we set $k = 2$ to limit the orbits of the system (11) into the working voltage scope of for operational amplifiers and analog multipliers. Electronic circuit of the system (11) is indicated in Fig. 12, where $C1 = C2 = C3 = 1\,\mu\text{F}$, $R1 = R3 = R5 = R6 = R8 = R9 = R14 = R15 = 10\,\text{k}\Omega$, $\text{R2} = 5\,\text{k}\Omega$, $R4 = R11 = R18 = 100\,\text{k}\Omega$, $R7 = R13 = R16 = 1\,\text{k}\Omega$, $R10 = R17 = 20\,\text{k}\Omega$, $R12 = 40\,\text{k}\Omega$, $V21 = 3\,\text{V}$. The circuit can implement the calculations of the system (11) which is the shrink version of the system (1). The orbits of the system (11) should be 1/2 times those of the system (1).

Circuit simulation results are shown in Fig. 13, where the scales of x- and y-axis are 5V. For $(a, b, c, d) = (1, 2, 1, 3)$, the attractors shown on oscilloscope in the circuit simulations are coincide with those of Fig. 1 obtained by numerical simulations. Because we set $k = 2$, the orbits of Fig. 13 are 1/2 times those of Fig. 1.

For $(a, b, c, d) = (1, 5, 1, 3)$, we change $R2$ to $2\,\text{k}\Omega$ and keep others no change. Its circuit simulation results are shown in Fig. 14 which is similar to Fig. 2 obtained by numerical simulations.

Furthermore, we set the shrink version of the system (10) with control parameter u and ratio parameter k as follows:

$$\begin{cases} \dot{x} = -ax + by \\ \dot{y} = -kxz + u/k \\ \dot{z} = ckx^2 + kxy - d/k \end{cases} \tag{12}$$

where $k \neq 0$. Obviously, orbits of the system (12) and those of the system(10) are of the same shape. The circuit diagram of the system (12), shown in Fig. 15, is formed by adding the resistor R19 and the voltage source VC on the basis of Fig. 14. We set $R19 = 40\,\text{k}\Omega$ and remain other resistors no change, so $u = \text{VC}$, $(a, b, c, d) = (1, 2, 1, 3)$ and $k = 2$. The orbits of

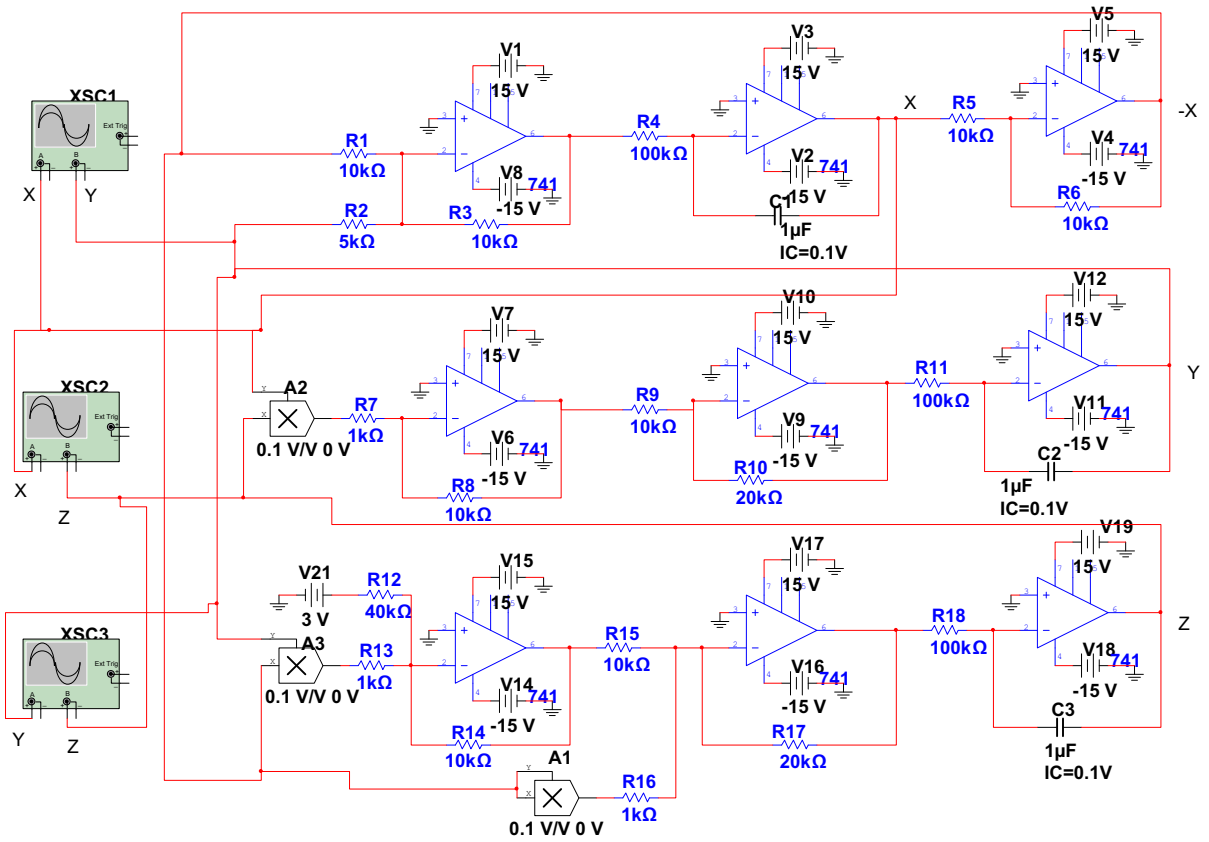

Fig. 12 Circuit diagram for the system (11) that is the shrink version of the system (1)

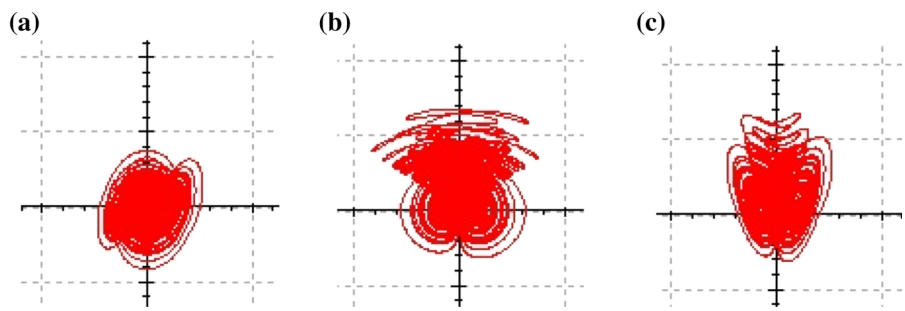

Fig. 13 Phase diagrams for $(a, b, c, d) = (1, 2, 1, 3)$ shown on oscilloscope whose scales of x- and y-axis are 5 V: **a** x–y, **b** y–z, **c** x–z

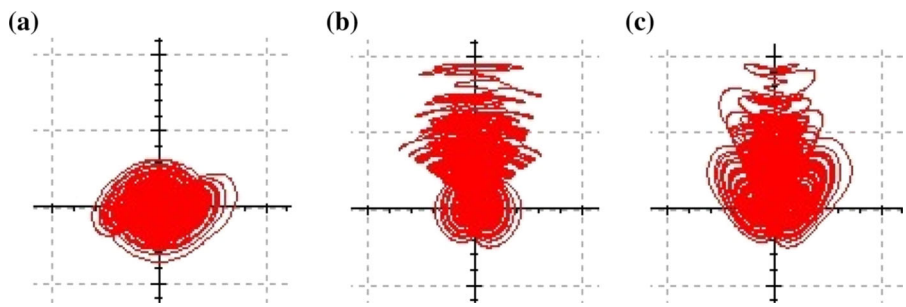

Fig. 14 Phase diagrams for $(a, b, c, d) = (1, 5, 1, 3)$ shown on oscilloscope whose scales of x- and y-axis are 5 V: **a** x–y, **b** y–z, **c** x–z

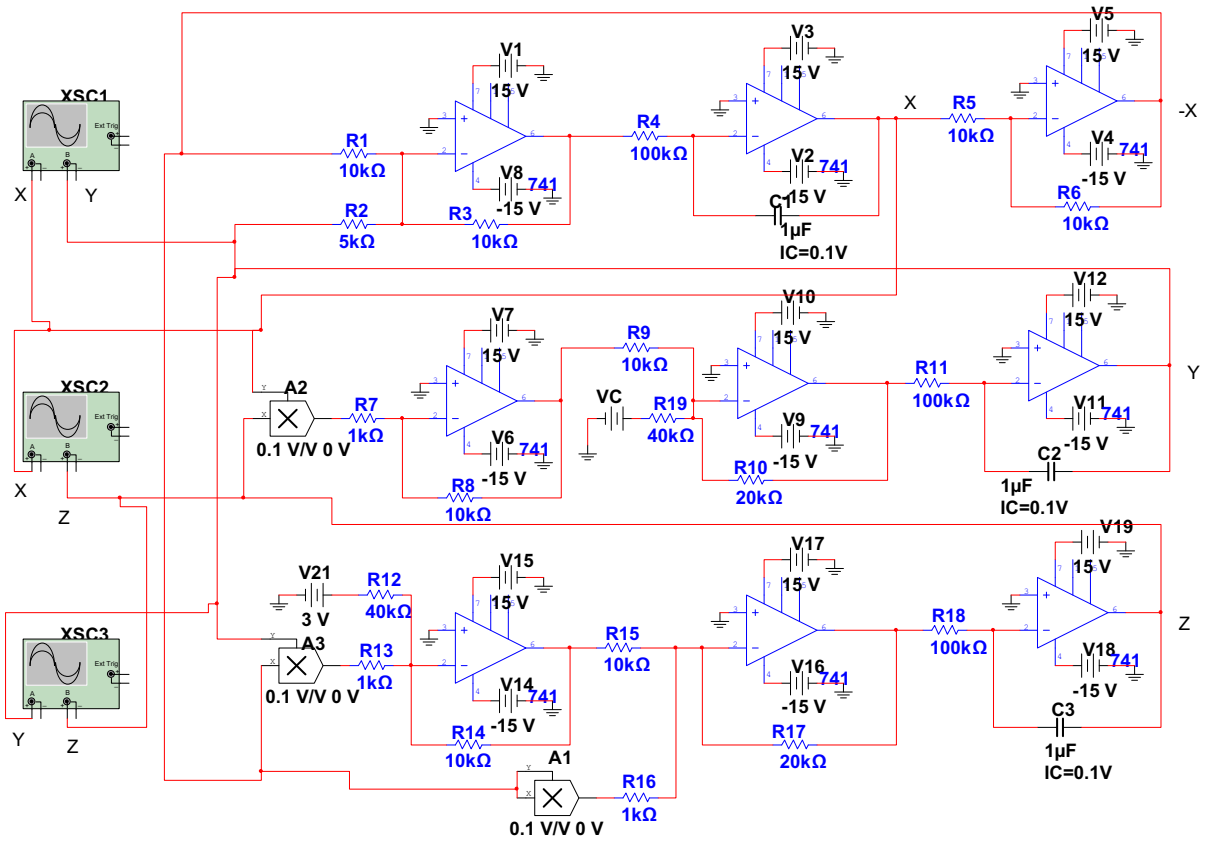

Fig. 15 Circuit diagram for the system (12) that is the shrink version of the controlled system (10)

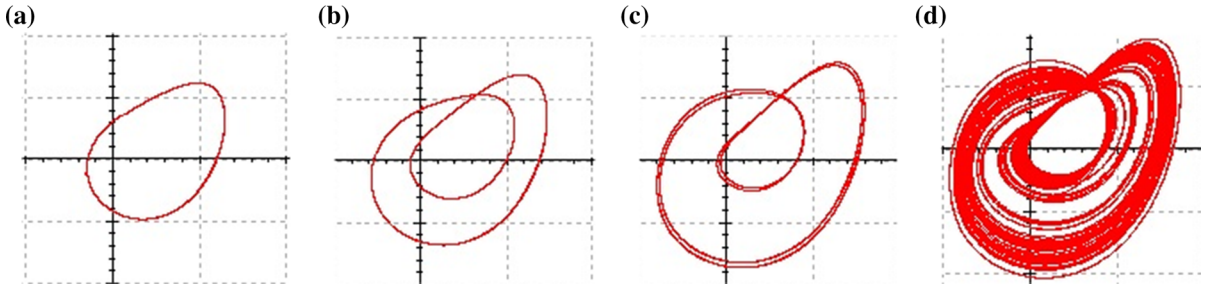

Fig. 16 x–y phase diagrams of the system (12) shown on oscilloscope whose scales of x- and y-axis are 1 V: **a** $u = \mathrm{VC} = 2.7$, **b** $u = \mathrm{VC} = 2.2$, **c** $u = \mathrm{VC} = 1.64$, **d** $u = \mathrm{VC} = 1.62$

the system (12) should be 1/2 times those of the system (10).

Circuit simulation results of Fig. 15 with different voltage source VC are shown in Fig. 16, where the scales of both x- and y-axis are 1V. We can roughly see that the orbits shown in Fig. 16 are approximately 1/2 times those shown in Fig. 10. That is to say, the circuit simulation results of the system (12), which is the shrink version of the controlled system (10), coincide well with the numerical simulation results of the system (10).

In order to compare the circuit simulation results with the numerical simulation results more specifically, we take the following example. We choose 10 groups of sample data from the circuit simulation results of the controlled system (12) with $u = 2.7$ and list the

Table 1 (x, y, z) sample data of the circuit simulations of Fig. 15 with $u = 2.7$

No.	x	y	z
1	1.0088	1.2434	0.7575
2	1.1222	−0.2363	2.4084
3	1.1550	1.1715	1.1330
4	1.1667	1.1585	1.1719
5	1.2096	1.0946	1.3316
6	1.2370	1.0337	1.4542
7	1.2756	0.3660	2.1809
8	1.2910	0.7506	1.8537
9	1.1410	−0.1870	2.4013
10	1.0928	−0.3071	2.4146

Table 2 $(x'/2, y'/2, z'/2)$ sample data of the numerical simulations of the system (10) with $u = 2.7$

No.	$x'/2$	$y'/2$	$z'/2$
1	1.0088	1.2305	0.7902
2	1.1203	−0.2383	2.4017
3	1.1550	1.1769	1.1153
4	1.1667	1.1657	1.1513
5	1.2100	1.1026	1.3124
6	1.2370	1.0167	1.4702
7	1.2756	0.3531	2.1858
8	1.2910	0.7711	1.8262
9	1.1410	−0.1983	2.4040
10	1.0928	−0.3086	2.4104

(x, y, z) in Table 1. Accordingly, we also choose 10 groups of sample data (x', y', z') from the numerical simulation orbits of the system (10) with $u = 2.7$, multiply them with 1/2 and list the $(x'/2, y'/2, z'/2)$ in Table 2. The (x, y, z) shown in Table 1 and the $(x'/2, y'/2, z'/2)$ listed in Table 2 should be very similar if the circuit simulation results coincide well with the numerical simulation results.

By comparing Tables 1 and 2, we can see that the (x, y, z) sample data of the numerical simulations are very close to the $(x'/2, y'/2, z'/2)$ sample data of the circuit simulations. That is to say, the circuit simulation results of the controlled system (12) which is the shrink version of the system (10) are roughly 1/2 times the orbits of the system (10), for $k = 2$ and $u = 2.7$.

From the above analyses, we can conclude that the results of circuit simulations are consistent well with those of the numerical simulations.

6 Conclusions

A six-term three-dimensional autonomous chaotic system with fan-shaped Poincaré maps is proposed. Theoretical analyses and numerical simulations prove that the proposed simple system with only six terms can keep complex chaotic behaviors within a wide range of parameters. Besides, circuit simulations testify that the system can be realized by electronic circuits. Results of numerical simulations and circuit simulations coincide with each other perfectly.

As we know, chaotic systems with wide-range parameters are usually welcome in some engineering applications, such as secure communications, information security, information hiding. Therefore, the proposed three-dimensional chaotic system featured by simple structure and wide-range parameters can find its way in many application fields. It deserves further detailed investigations on its theoretical analyses and simulations.

Acknowledgments This work was supported by the National Natural Science Foundations of China (Nos. 21310018 and 61077030), the Science and Technology Research Program for the International Cooperation of Guangdong Province of China (2010B050900016). The authors are grateful to the reviewers for their valuable comments on the paper.

References

1. Edward, O.: Chaos in Dynamical Systems, 2nd edn. Cambridge University Press, Cambridge (2002)
2. Lorenz, E.N.: Deterministic nonperiodic flow. J. Atmos. Sci. **20**, 130–141 (1963)
3. Rössler, O.E.: An equation for continuous chaos. Phys. Lett. A **57**, 397–398 (1976)
4. Genesio, R., Tesi, A.: Harmonic balance methods for the analysis of chaotic dynamics in nonlinear systems. Automatica **28**, 531–548 (1992)
5. Sprott, J.C.: Some simple chaotic flows. Phys. Rev. E **50**, 647–650 (1994)
6. Sprott, J.C., Linz, S.J.: Algebraically simple chaotic flows. Int. J. Chaos Theory Appl. **5**, 3–22 (2000)
7. Chen, G., Ueta, T.: Yet another chaotic attractor. Int. J. Bifurc. Chaos **9**, 1465–1466 (1999)
8. Lü, J.H., Chen, G.R.: A new chaotic attractor coined. Int. J. Bifurc. Chaos **3**, 659–661 (2002)

9. Liu, C., Liu, T., Liu, L., Liu, K.: A new chaotic attractor. Chaos Solitons Fractals **22**, 1031–1038 (2004)
10. Yu, S., Lu, J., Chen, G.: Theoretical design and circuit implementation of multidirectional multi-torus chaotic attractors. IEEE Trans. Circuits Syst. I Regul. Pap. **54**, 2087–2098 (2007)
11. Munmuangsaen, B., Srisuchinwong, B.: A new five-term simple chaotic attractor. Phys. Lett. A **373**, 4038–4043 (2009)
12. Ling, L., Chongxin, L., Yanbin, Z.: Experimental verification of a four-dimensional Chua's system and its fractional order chaotic attractors. Int. J. Chaos Theory Appl. **19**, 2473–2486 (2009)
13. Shijian, C., Guoyuan, Q., Zengqiang, C.: A four-wing hyperchaotic attractor and transient chaos generated from a new 4-D quadratic autonomous system. Nonlinear Dyn. **59**, 515–527 (2010)
14. Li, X., Ou, Q.: Dynamical properties and simulation of a new Lorenz-like chaotic system. Nonlinear Dyn. **65**, 255–270 (2011)
15. Zhang, X., Zhu, H., Yao, H.: Analysis of a new three dimensional chaotic system. Nonlinear Dyn. **67**, 335–342 (2012)
16. Kim, D., Chang, P.H.: A new butterfly-shaped chaotic attractor. Results Phys. **3**, 14–19 (2013)
17. Chang, P.H., Kim, D.: Introduction and synchronization of a five-term chaotic system with an absolute-value term. Nonlinear Dyn. **73**, 311–323 (2013)
18. Kim, D., Chang, P.H., Kim, S.: A new chaotic attractor and its robust function projective synchronization. Nonlinear Dyn. **73**, 1883–1893 (2013)
19. Ping, Z., Kun, H.: A new 4-D non-equilibrium fractional-order chaotic system and its circuit implementation. Commun. Nonlinear Sci. Numer. Simul. **19**, 2005–2011 (2014)
20. Banihasan, M., Bakhtiari-Nejad, F.: Chaotic vibrations in high-speed milling. Nonlinear Dyn. **66**, 557–574 (2011)
21. Wiggins, S.: The dynamical systems approach to Lagrangian transport in oceanic flows. Annu. Rev. Fluid Mech. **37**, 295–328 (2005)
22. Klonowski, W.: Chaotic dynamics applied to signal complexity in phase space and in time domain. Chaos Solitons Fractals **14**, 1379–1387 (2002)
23. Yang, H., Jiang, G.P.: Reference-modulated DCSK: a novel chaotic communication scheme. IEEE Trans. Circuits Syst. II Express Briefs **60**, 232–236 (2013)
24. Volos, C.K., Kyprianidis, I.M., Stouboulos, I.N.: Image encryption process based on chaotic synchronization phenomena. Signal Process. **93**, 1328–1340 (2013)